Experimental Feedback Control of Flow Induced Cavity Tones

Randolph H. Cabell*, Michael A. Kegerise†, David E. Cox‡, Gary P. Gibbs*
NASA Langley Research Center, Hampton, VA 23681

An experimental study of the application of discrete-time, linear quadratic control design methods to the cavity tone problem is described. State space models of the dynamics from a synthetic jet actuator at the leading edge of the cavity to two pressure sensors in the cavity were computed from experimental data. Variations in model order, control order, control bandwidth, and properties of a Kalman state estimator were studied. Feedback control reduced the levels of multiple cavity tones at Mach 0.275, 0.35, and 0.45. Closed loop performance was often limited by excitation of sidebands of cavity tones, and creation of new tones in the spectrum. State space models were useful for explaining some of these limitations, but were not able to account for non-linear dynamics, such as interactions between tones at different frequencies.

Introduction

THE generation of tones by flow over a rectangular cavity is a well known phenomenon which affects landing gear and weapons bays on aircraft. The sound pressure levels of the tones can be very high, which can create a noise problem inside the aircraft and can destroy delicate instrumentation in the cavity itself. While the reduction of the noise levels is an important issue, the cavity tone problem is also an interesting testbed for active flow control studies. Active control of flow around an airfoil has been proposed as an alternative to traditional control surfaces on future aircraft configurations. There are several issues found in the cavity tone problem which have relevance to broader flow control problems, including: limited actuator authority, non-linearities, and a lack of physics-based models which can be used for control design.

There has been previous work on actively controlling cavity tones, although much of it involved manual tuning of the gain and delay of simple feedback loops at select frequencies of interest.[1–5] These works demonstrated reductions of 10-20 dB in the sound pressure level (SPL) of a single tone, and modest success at reducing multiple tones. Although manual tuning of feedback loops is impractical for a general flow control problem, these works were valuable for several reasons: they demonstrated the potential of feedback control, showed the relative time invariance of the phenomenon, and provided useful data on the suitability of different actuators.

More automated approaches to control cavity tones have also been studied. An adaptive feedforward control method was described by Williams,[3] in which a pressure transducer in the cavity was used as a reference signal. The approach reduced a single tone by 15 dB, but could not suppress multiple tones. A linear quadratic regulator was used to control a single mode resonance at low Mach numbers (<0.15),[6] and an adaptive feedback approach has also been tested by the same author,[7] based on the adaptive disturbance rejection algorithm.[8] In the adaptive work, the parameters of a feedback controller were adjusted online to maximize disturbance rejection. The controller reduced a single tone by 10 dB, but was not successful at reducing multiple tones, which may have been due to actuator limitations rather than the algorithm. More recent work proposed the development of a physics-based model that could be used for feedback control design.[4,5] The generation of tones in the cavity was modeled as a series of transfer functions which included feedback paths. Time delays due to disturbance propagation downstream in the shear layer and acoustic propagation upstream in the cavity were dominant features of this model. While a physics-based model is useful for physical insight, no such model is currently available with the accuracy needed to design and implement a feedback controller.

The current paper describes the application of discrete-time linear quadratic control design methods, augmented with frequency shaping,[9] to the cavity tone problem. These methods were chosen because they are well understood and can be based directly on experimentally identified models of the system being controlled. In addition, this approach can be readily extended to a predictive control method which integrates model identification and control design,[10] leading to a fully adaptive controller.

Because this was an initial study of the approach, the simplifying assumptions of linearity and time invariance were made. The approach was based on

*Structural Acoustics Branch
†Flow Physics and Control Branch
‡Guidance and Control Branch

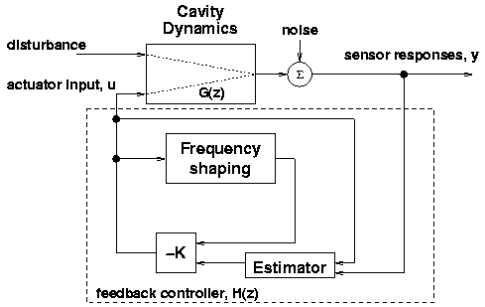

Fig. 1 Block diagram of control system

treating the problem as a broadband control problem, rather than one of discrete tones. Broadband models of the cavity system were computed from experimentally measured data. While the resulting controller is not explicitly derived from physics-based insights, the goal of this work was to study the suitability of experimentally based control design. It is hoped that these results will be useful for guiding the development of physics-based models and subsequent control designs.

Feedback control tests were conducted on a cavity located in the Probe Calibration Tunnel at NASA Langley Research Center. A synthetic jet, positioned at the leading edge of the cavity, was used as a control actuator. Two dynamic pressure transducers were located in the cavity and were used as feedback error sensors. Over 260 control designs were tested, involving variations in model order, controller bandwidth, estimator design, and controller order. Tests were conducted at flow speeds of Mach 0.275, 0.35, and 0.45.

The paper begins with a description of the system identification and control design methods. The Experimental Setup section contains descriptions of the tunnel, cavity, and control transducers. The Results section describes an initial analysis of the test data, including the cavity response with no control, and transfer function models of the control system. Example closed loop results at each flow speed are discussed and compared with models of the closed loop transfer function. The paper ends with results which illustrate the limitations of linear models for this problem.

Analysis

Details of the control design methodology, which was based on linear quadratic control methods, are described here. This includes identification of a state space cavity model, design of a state estimator, and computation of the feedback gains.

For the purpose of control design, the block diagram representation of the cavity and feedback control system shown in Fig. 1 is helpful. The dynamics of the cavity were assumed to be linear and time-invariant (LTI), allowing for an LTI model to be fit to experimentally measured data and the subsequent design of an LTI control law. Although an approximation, this model did reproduce the spectral response of the sensors as seen from the actuator, and seemed to remain accurate over several hours of testing.

The block diagram represents the cavity as a mapping from inputs to outputs. The inputs consist of an unknown disturbance which feeds into the shear layer at the cavity's leading edge, and an input due to a control actuator. The outputs consist of pressure transducers in the cavity. The disturbance in this diagram represents any input to the shear layer/cavity system other than the control actuator, such as upstream flow disturbances or acoustic disturbances in the cavity which couple into the shear layer. These disturbances are difficult to model and could not be determined from the current experimental data. Therefore all control designs were posed as disturbance rejection from the actuator itself, and not rejection of a known disturbance source. Nonetheless, disturbance rejection through the actuator still provides for an appropriate general trend because active control will add damping and reduce peak responses, but it does not allow for a direct comparison of predicted and experimental results.

A state space model was assumed for the dynamics from the actuator input to the sensor responses. If the actuator input at sample time k is written u_k, and the vector of sensor responses is written $\mathbf{y}_k^c$ (assuming multiple pressure transducers are located in the cavity), the state space model can be written

$$\begin{aligned} \mathbf{x}_{k+1}^c &= \mathbf{A}^c \mathbf{x}_k^c + \mathbf{B}^c u_k \\ \mathbf{y}_k^c &= \mathbf{C}^c \mathbf{x}_k^c + \mathbf{D}^c u_k \end{aligned} \tag{1}$$

where $\mathbf{x}_k^c$ is the state vector of the cavity model. The superscript c is used to differentiate this model from a frequency dependent effort weighting model discussed later.

The matrices $\mathbf{A}^c, \mathbf{B}^c, \mathbf{C}^c, \mathbf{D}^c$ were determined through system identification. For the present work, the matrices were computed from experimentally measured data using a modified version of the eigensystem realization algorithm.[11,12] This algorithm computes state space matrices with a specified number of degrees of freedom from time domain input-output data. The input-output data were collected by driving the control actuator with a broadband signal and recording the corresponding sensor responses. Because the flow across the cavity is a significant aspect of the overall cavity dynamics, the input-output data was always collected at the flow speed for which control was to be applied.

The number of degrees of freedom of the state space model, or model order, was chosen so the identified model reproduced the spectral responses of the sensors as seen from the control actuator. High model orders, ranging from 150 to 200 states, were generally needed for the eigensystem realization algorithm to accurately reproduce the dynamics near the cavity tones. For control design the order was generally reduced to

approximately 60 states in order to reduce over parameterization and obtain a controller more suitable for real-time implementation. Model reduction was done using balanced realization truncation [9, Ch. 10]. Further model reduction, below 60 states, would be desirable since the parameters of a smaller model can be more easily related to the underlying physics of the problem, in addition to being easier to implement in hardware. However, a detailed study to determine the minimum model and controller order was not done in this experiment.

A frequency shaping technique was used to restrict control energy to a frequency range containing the cavity tones. This helped reduce spillover and actuator saturation due to out-of-bandwidth control effort. The approach is based on augmenting the plant model in Eq. 1 with filter dynamics, $\mathbf{A}^f, \mathbf{B}^f, \mathbf{C}^f, \mathbf{D}^f$ to create an additional plant output.[9] For the current work a bandstop filter was used, where the stopband contained the cavity tones. This filter shape imposed a higher effort penalty in the passband regions, at frequencies above and below the cavity tones. The upper and lower corner frequencies of the bandstop filter were control design parameters. Combining the cavity and frequency shaping models into one state space system yields

$$\begin{aligned} \begin{bmatrix} \mathbf{x}^c \\ \mathbf{x}^f \end{bmatrix}_{k+1} &= \begin{bmatrix} \mathbf{A}^c & 0 \\ 0 & \mathbf{A}^f \end{bmatrix} \begin{bmatrix} \mathbf{x}^c \\ \mathbf{x}^f \end{bmatrix}_k + \begin{bmatrix} \mathbf{B}^c \\ \mathbf{B}^f \end{bmatrix} u_k \\ \mathbf{x}_{k+1} &= \mathbf{A}\mathbf{x}_k + \mathbf{B}u_k \end{aligned} \tag{2}$$

for the combined state vector, and produces

$$\begin{aligned} \begin{bmatrix} \mathbf{y}^c \\ y^f \end{bmatrix}_k &= \begin{bmatrix} \mathbf{C}^c & 0 \\ 0 & \mathbf{C}^f \end{bmatrix} \begin{bmatrix} \mathbf{x}^c \\ \mathbf{x}^f \end{bmatrix}_k + \begin{bmatrix} \mathbf{D}^c \\ \mathbf{D}^f \end{bmatrix} u_k \\ \mathbf{y}_k &= \mathbf{C}\mathbf{x}_k + \mathbf{D}u_k \end{aligned} \tag{3}$$

for the combined outputs. The additional output, y^f, was penalized along with the pressure sensor outputs in the control cost function. This allowed a frequency dependent weighting to be applied to the control effort penalty, but did not introduce phase delay as would occur with in-line filtering of the actuator signal.

The controllers were designed to minimize the quadratic performance function

$$\begin{aligned} J &= \sum_{k=1}^{\infty} \mathbf{y}_k^T \mathbf{Q} \mathbf{y}_k + r u_k^2 \\ &= \sum_{k=1}^{\infty} \mathbf{x}_k^T \mathbf{C}^T \mathbf{Q} \mathbf{C} \mathbf{x}_k + (\mathbf{D}^T \mathbf{Q} \mathbf{D} + r) u_k^2 \end{aligned} \tag{4}$$

where the non-negative definite matrix $\mathbf{Q}$ defines the performance of the system, and r is a positive scalar that sets a frequency-independent control effort penalty. The optimal control corresponding to Eq. 4 is implemented as

$$u_k = -\mathbf{K}\mathbf{x}_k \tag{5}$$

A solution for the optimal controller, given the augmented plant model (Eqs. 2 and 3), $\mathbf{Q}$, and r, is well known[9] and is implemented in many engineering software packages.

In order to implement control as in Eq. 5, the state vector $\mathbf{x}_k$ is needed. However, the states produced by the system identification do not usually correspond to physically meaningful parameters, so the state vector cannot be measured and must instead be estimated from the measured responses, $\mathbf{y}_k^c$, and control input, u_k. Note that for the current problem, a portion of the state vector, $\mathbf{x}_k^f$, is strictly due to the effort weighting filters and is not part of the physical system. These states can be predicted without error from the actuator signal and in doing so this reduces the number of states which must be estimated.

A discrete Kalman estimator was used to obtain the cavity model state estimates. In estimating the state vector from control inputs and measured responses, the optimal Kalman estimator considers two sources of uncertainty: process noise, which includes disturbances at the input to the system and modeling inaccuracies, and measurement noise at the system output.[11] Output, or measurement, noise is shown in Fig. 1 as noise which enters the sensor response after the cavity. The relative levels of measurement and process noise determine the degree of trust the estimator puts in the sensor signals for state estimation. To simplify the estimator computation, both noise sources were assumed to be Gaussian and independent. In this case the important parameter for estimator design becomes the ratio of the measurement and process noise covariances. This ratio is usually unknown, so it is another design parameter in the control law, and along with the frequency weighting of control effort, has a significant effect on the bandwidth of the resulting controller.

To better illustrate the trade-offs in selecting parameters of the control law, the parameters are compared graphically in Fig. 2(a). The solid curve in Fig. 2(a) shows the magnitude of a cavity transfer function, specific details of which are presented in the Results section. If $\mathbf{Q}$ in Eq. 4 is the identity matrix, then this transfer function magnitude represents the performance output in the quadratic performance function. The dashed line in the plot represents the bandstop filter used as a frequency dependent control effort penalty. At low and high frequencies the control effort term lies well above the performance curve, hence the control effort term will dominate the cost function. The corresponding optimum controller will be of low gain in these frequency ranges. Within the stopband of the effort penalty, the floor of the stopband filter is set by the value r in Eq. 4. For the example in the figure, the performance curve dominates in the stopband, so the controller will be of high gain in this area.

Figure 2(b) illustrates the tradeoff between measurement and process noise in the Kalman state estimator.

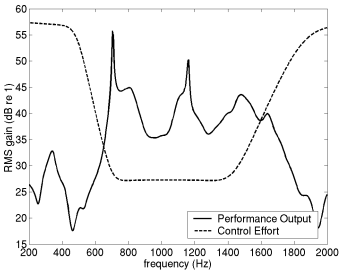

a) Performance vs. Control Effort

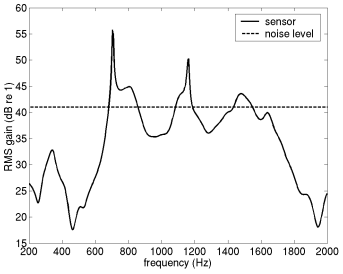

b) Process vs. Measurement Noise

Fig. 2 Graphical evaluation of trade-offs in control design parameters

The figure shows the same transfer function as in Fig. 2(a), but here the dashed line represents the ratio of the covariances of measurement noise to process noise. For this example, the relative levels of the two curves indicate that the sensor response is assumed to consist of random measurement noise for a large part of the spectrum. Only near peaks at 700, 1200, and 1500 *Hz* is the sensor response assumed to be due to the plant model. The Kalman estimator corresponding to this example would be of low gain where measurement noise dominates the sensor response. As a result, the state estimates in these frequency ranges would tend to zero, which has the effect of rolling off the gain of the controller. Therefore, a ratio of measurement to process noise which is constant with frequency tends to roll off the control gains as the plant's response rolls off.

It is often useful to predict the closed loop behavior of the control system without actually closing the loop in hardware. Using the notation from Fig. 1, $G(z)$ denotes the discrete time transfer function from actuator input to sensor responses. Likewise, $H(z)$ denotes the transfer function of the feedback controller. The transfer function for the closed loop system is written

$$\frac{Y(z)}{U(z)} = \frac{G(z)}{1 + G(z)H(z)} \tag{6}$$

This equation provides a way to check the stability and performance of the system. Since there will be errors in the state space model of the plant, the predicted performance is only an approximation of the actual performance.

The sensitivity of the closed loop control system is also a useful analysis tool. The sensitivity is defined as the transfer function from random noise in the sensor to the sensor response itself. The random noise input is shown in Fig. 1 as summing with the sensor response due to the cavity. The sensitivity, written as a transfer function of sensor response, $Y(z)$, for a given random noise input, $N(z)$, is

$$\frac{Y(z)}{N(z)} = \frac{1}{1 + G(z)H(z)} \tag{7}$$

The sensitivity quantifies how sensor noise is amplified or attenuated by the feedback control system.[9] A sensitivity magnitude greater than 1 (or 0 dB) indicates sensor noise amplification, whereas a magnitude less than 1 indicates an attenuation. When disturbance rejection is the primary concern, as for the cavity problem, the sensitivity should be as small as possible in frequency ranges where the disturbance is to be minimized.

Experimental Setup

The wind tunnel facility, cavity model, and transducers used to implement feedback control are described in this section.

Wind Tunnel Facility

The experiments were conducted in the NASA Langley Probe Calibration Tunnel (PCT). The PCT is typically operated as an open-jet pressure tunnel with independent control of stagnation pressure, stagnation temperature, and free stream velocity. The stagnation pressure and temperature ranges for the facility are 13.8 kPa to 1034 kPa and 255 K to 367 K, respectively. For the current experiments, the facility was fitted with a subsonic nozzle that contracts from a circular inlet to a 50.8 mm by 152.4 mm exit. A straight duct section of length 0.6 m was attached to the nozzle exit and was terminated with a small-angle diffuser. The free stream Mach number range for the present tunnel configuration was 0.04 to 0.8.

Cavity Model

A rectangular cavity model was installed in the ceiling of the straight duct section of the PCT. The floor of the duct section was a foam filled baffle which minimized reflections of acoustic waves radiated by the cavity. The cavity model had a fixed length, $\ell = 152.4$ mm, and a variable depth, d which was fixed to 30.48 mm, for an ℓ/d ratio of 5. The cavity model spanned the width of the test section ($w = 50.8$ mm) to provide an un-obscured view of the cavity shear layer for optical diagnostics. A schematic of the cavity (drawn inverted from its installed position for clarity) is shown in Fig. 3, with actuator and sensor locations indicated.

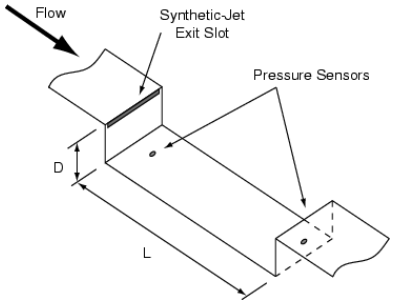

Fig. 3 Schematic of cavity

Sensors

The cavity model was instrumented with a pair of piezoresistive pressure transducers (Endevco model 8510B-2). The sensors had a nominal sensitivity and bandwidth of 2.2×10^{-5} *V/Pa* and 14 *kHz*, respectively. One sensor was located in the floor midplane, 18 *mm* downstream from the cavity front wall. The second sensor was located in the midplane of the rear cavity wall, 19 *mm* from the cavity trailing edge. The signals from the sensors were pre-amplified and low-pass filtered with 6th order elliptic filters with a corner frequency of 3 *kHz*.

Actuator

It is important to minimize or eliminate disturbances which are fed into the shear layer at the cavity leading edge by acoustic feedback. The point at which actuation is applied is critical; actuation at the cavity leading edge, where the shear layer is most sensitive, should minimize the required control effort. Recent attempts at cavity control have adopted this approach for actuation.[2,3,7]

A piezo-driven synthetic jet was chosen as the actuator for the current study. The exit of the synthetic jet actuator was a rectangular slot, 44.5 *mm* long by 0.5 *mm* high, located just below the cavity leading edge. The exit flow was oriented such that it introduced disturbances parallel to the free stream direction. This design was based on the recent results of Williams *et al.*,[2,3] that suggest this orientation is optimal.

Benchtop measurements of the actuator output velocity in a quiescent medium revealed the peak velocity at the slot exit was ≥ 15 *m/sec* over a frequency range of 600 to 1500 *Hz*. However, the slot exit boundary conditions undoubtedly change when placed in the cavity environment, which is expected to cause the magnitude of the exit velocity to change. No attempt was made to characterize the output velocity of the actuator while operating in the cavity environment with flow. The control signal sent to the actuator was not filtered since the actuator's response naturally rolled off above 3 *kHz*.

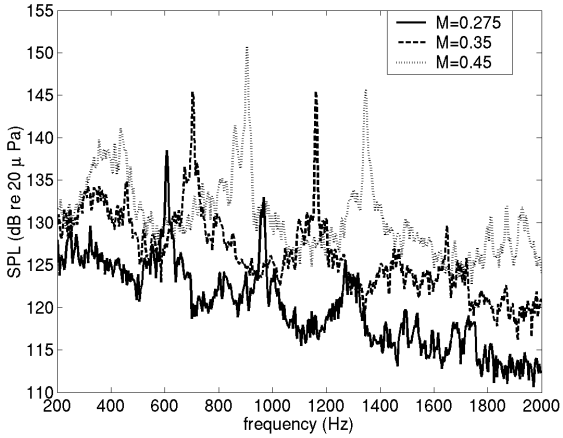

Fig. 4 Response of rear pressure transducer at three flow speeds.

Control Hardware

The feedback controllers were implemented on a floating point digital signal processor (DSP). The DSP was also used to collect input-output data for system identification. This ensured an accurate measurement of all gains and delays in the control path. The sample rate for all control designs discussed here was 7500 *Hz*.

Results and Discussion

Closed loop performance data was collected over a four day period for over 260 control designs. Variations in model order (the size of the identified state space model of the cavity dynamics), control order (the model order after internal balancing and state reduction), control bandwidth, and sensor noise variance in the state estimator were tested. The results presented here were selected to validate the combined experimental system identification and optimal control design procedure.

This section begins with the response of the rear pressure transducer at the three flow speeds of interest. Next, models of the identified transfer function from synthetic jet input to sensor response are described. This is followed by examples of closed loop results at each flow speed. The section ends with a discussion of results from Mach 0.35 which illustrate the complexity of the cavity tone problem.

Open Loop Response

The response of the rear pressure transducer at three flow speeds is shown in Fig. 4. The plots show the autospectrum of the transducer output, computed from 5.3 sec of data with a frequency spacing of 3.7 *Hz*. At each flow speed, the sensor response is dominated by two tones. The basic flow physics responsible for these tones were first described by Rossiter,[13] hence the tones are commonly referred to as the Rossiter modes or Rossiter tones of the cavity.

The tones in Fig. 4 correspond to the second and

third Rossiter modes for the cavity at each flow speed. Table 1 compares measured and predicted frequencies for these tones. The predictions were computed using a modified Rossiter equation,[14] where κ, the phase speed of the downstream propagating instability wave was assumed to be 0.66 times the freestream velocity, and the phase lag term, α, was 0.25.

Table 1 Measured vs. predicted frequencies (Hz) of the 2nd and 3rd Rossiter modes

Mach	Mode 2		Mode 3	
#	Meas.	Pred.	Meas.	Pred.
0.275	609	604	965	950
0.35	704	737	1160	1159
0.45	903	898	1343	1411

Open Loop Transfer Function

The control methodology assumed that an accurate state space model of the transfer function from actuator input to sensor outputs was available. This model was computed from measured input-output data where the actuator was driven with a random signal with a bandwidth of 100-3700 *Hz*. Because the data were collected with the tunnel operating, the coherence from driving signal to sensor response was low. At all three flow speeds the coherence was less than 0.05 below 500 Hz and above 3 kHz, where the synthetic jet had little control authority. In between those frequencies, the coherence went down with flow speed: < 0.5 at Mach 0.275, < 0.4 at Mach 0.35, and < 0.2 at Mach 0.45. To compensate for the low coherence, long time records (10 seconds) were collected for system identification.

Examples of identified state space models at the three flow speeds are shown in Fig. 5. The magnitude of the transfer function from actuator input to rear pressure sensor response is shown. The number of states in each model is indicated in the figure legend, and varied from 80 at Mach 0.275 to 60 states at Mach 0.35 and 0.45.

The transfer function magnitude offers insight into using the synthetic jet as a broadband actuator. At the two higher flow speeds, dynamics near the Rossiter modes dominate the transfer function. The actuator authority drops off by 20 dB or more at frequencies away from the Rossiter modes. At the lowest flow speed there are significant dynamics between the Rossiter modes. For example, at Mach 0.275, the transfer function peaks at 800 *Hz*, which lies between the two Rossiter modes at 609 and 965 *Hz*. This peak, which is visible to some degree at all three flow speeds, is most likely due to a resonance of the piezoelectric actuator in the synthetic jet. In all three cases the transfer function rolls off significantly at high and low frequencies.

The transfer function models seemed to remain accurate over several hours of testing at a given flow

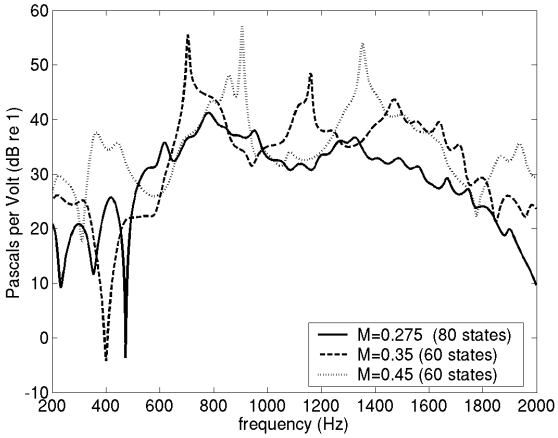

Fig. 5 Modeled transfer function magnitude from actuator to rear pressure transducer at three flow speeds

speed. During the experiments, a single state space model was used to generate a suite of feedback control designs. Testing each design took a few minutes, so the last few controllers in a suite were sometimes tested a few hours after the transfer function model had been computed. Fortunately, none of the results indicated that closed loop performance was related to the time elapsed since system identification. This suggests that both the tunnel conditions and tone generation mechanism did not change significantly over a few hour period.

Closed Loop Results

Autospectra of the rear sensor response for control and no control cases are shown in Figs. 6(a), 6(c), and 6(e). These three cases, one at each flow speed, illustrate some of the best reductions obtained during the four days of testing. Multiple tones were reduced at each flow speed, and a slight reduction in the broadband level was obtained at the two higher flow speeds. Similar reductions were obtained at the front sensor, but for simplicity only the rear sensor response will be discussed here.

At Mach 0.275, the three most prominent tones in the spectrum, corresponding to the 2nd, 3rd, and 4th Rossiter modes, were reduced by 7.8 dB, 6.9 dB, and 4.1 dB, respectively. However, the controller excited a new tone above the 4th mode at 1550 *Hz*. At Mach 0.35 the 2nd and 3rd Rossiter modes were reduced by 7.9 dB and 10.1 dB, respectively. The sidebands near the 3rd mode at 1160 *Hz* were increased by the controller. A slight reduction in the broadband level is apparent between the two tones. The peak in the open loop response at 460 *Hz* was caused by a difference interaction due to quadratic coupling between the two Rossiter modes. As the peak levels of those two tones dropped, the peak level of the 460 *Hz* tone also dropped. Smaller reductions were obtained at Mach 0.45, where the 2nd Rossiter mode was re-

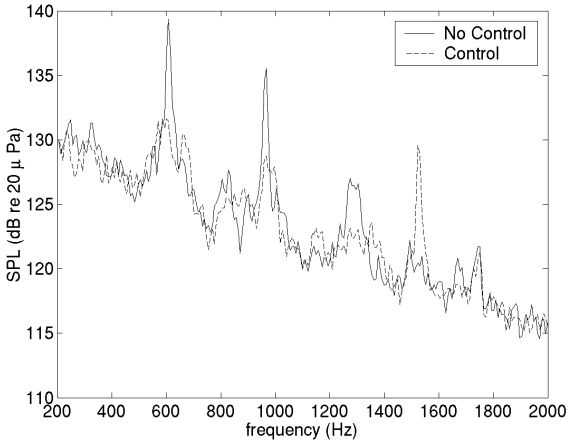

a) Mach 0.275 (Run 1355): Rear sensor response with and without control.

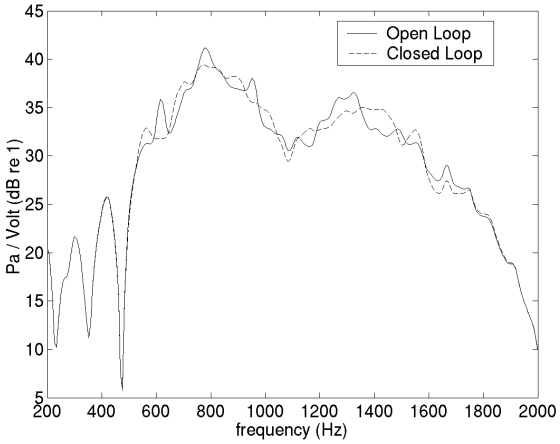

b) Mach 0.275 (Run 1355): Open and closed loop transfer function from actuator to rear sensor.

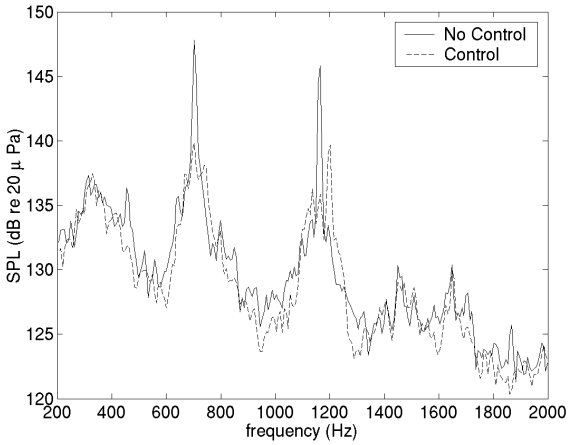

c) Mach 0.35 (Run 1428): Rear sensor response with and without control.

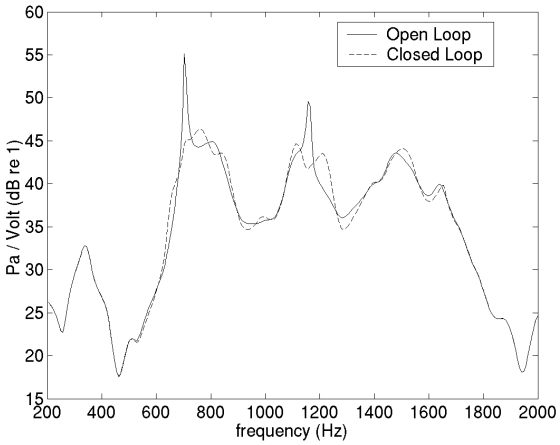

d) Mach 0.35 (Run 1428): Open and closed loop transfer function from actuator to rear sensor.

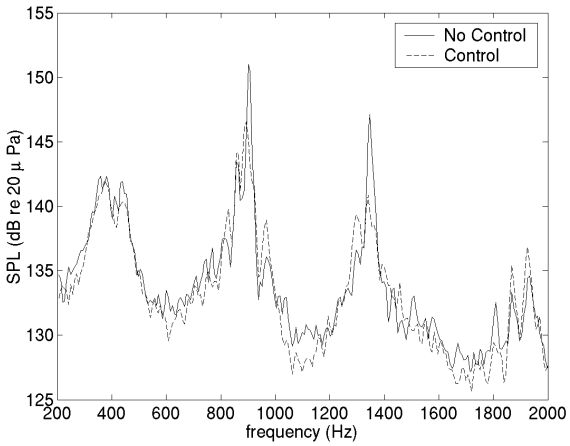

e) Mach 0.45 (Run 1535): Rear sensor response with and without control.

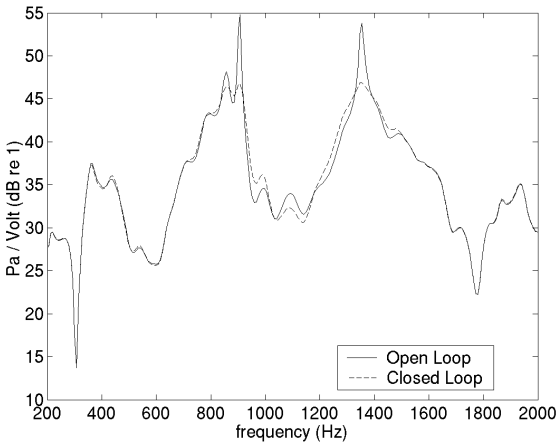

f) Mach 0.45 (Run 1535): Open and closed loop transfer function from actuator to rear sensor.

Fig. 6 Measured and modeled control performance at three flow speeds

duced by 5.0 dB and the 3rd mode was reduced by 6.5 dB. A slight reduction in the broadband level is evident between the two tones.

The control and estimator design parameters for these three cases are listed in Table 2. The first column gives the time of day that each controller was tested; for convenience this is also used as a run number. The number of states for the full state space model and the reduced state space model, from which the controller was designed, are listed in columns 3 and 4. Columns 5-8 give the properties of the bandstop filter used to penalize control effort. The stopband and passband levels are listed in units of dB of transfer function gain, corresponding to the transfer functions shown in Fig. 5. These units make it easier to compare the effort penalty filter to the transfer function gain, as in the discussion of Fig. 2(a). The sensor noise variance used to compute the state estimator, listed in the last column of the table, is also expressed in units of transfer function gain.

Open and closed loop transfer functions from the actuator input to the rear sensor are shown in Figs. 6(b), 6(d), and 6(f). The solid curve shows the open loop transfer function, $G(z)$, while the dashed curve shows the closed loop transfer function computed using Eq. 6. In each case a state space model, such as one of those shown in Fig. 5, was used for the open loop transfer function. These curves can't be directly compared with the measured data since the measured results correspond to a different transfer function driven by an unknown disturbance. Nonetheless, if trends in the closed loop model match trends in the measured results, it would validate the state space model and thereby validate the assumption of linearity. It is also useful to know if the closed loop transfer function can be used to optimize the control design, without having to close the loop and collect data on every design.

At all three flow speeds the closed loop model shows varying amounts of disturbance attenuation and amplification in different frequency ranges. Specifically, the model shows disturbance attenuation whenever the dashed line is less than the solid line. At Mach 0.275, Figure 6(b) indicates the controller will attenuate the disturbance near the Rossiter modes at 610, 960, and 1250 *Hz*, which agrees with the measured results. The closed loop model also shows disturbance amplification above 610 *Hz*, below 1200 *Hz*, and near 1550 *Hz*. The measured results verify that with control on, the sensor response increased at these frequencies. The magnitude of disturbance amplification seen in the measured results near 1550 *Hz* is curious, since the prediction doesn't suggest such a large amplification. Assuming a linear system and a constant disturbance, the tone at 1550 *Hz* could be due to an error in the state space model.

Trends in the open and closed loop transfer functions in Figs. 6(d) and 6(f) also agree with measured results. At Mach 0.35, Fig. 6(d) shows a slight amplification of the disturbance just above the cavity tone at 700 *Hz*, and the measured results agree. Amplification is also predicted and was measured above and below the mode at 1160 *Hz*. The measured reduction at 460 *Hz* was not predicted by the linear model, which is to be expected since this tone was due to a non-linear effect.

Peak-splitting, peaking, and non-linear dynamics

In addition to demonstrating reductions of multiple cavity tones, the preceding results also show "peak splitting" and generation of secondary peaks, or "peaking," to use terminology from the combustion control community.[15] Peak splitting refers to the excitation of sidebands of a tone, and can be seen in Fig. 6(c) near 1200 Hz. Peaking, or generation of a secondary peak, is evident in Fig. 6(a), near 1550 Hz. This behavior appears to be common in feedback control of cavity tones.[3–5,7]

To a certain extent the peak-splitting can be explained by looking at the gain and phase of the closed loop system, using the expression given in Eq. 6. For example, the magnitudes of the closed loop transfer functions in Figs. 6(b), 6(d), and 6(f) all show some disturbance amplification in the sidebands of the cavity tones. This can be attributed to two factors: the large control gain concentrated in a narrow frequency band about the cavity tones, and the significant time delay from actuator input to sensor response. Previous works have discussed this tendency in greater detail, in the context of the cavity tone problem and for controlling combustion instabilities.[5,15,16]

Notwithstanding the agreement between the modeled and measured results, there are non-linearities in the cavity problem which deserve consideration. To illustrate, results from a second control design at Mach 0.35, labeled Run 1418, are shown in Fig. 7(a) with results from Run 1428 discussed previously. The Run 1418 controller reduced the two Rossiter modes without increasing the sidebands, but it generated a secondary tone at 1660 Hz. Instead of comparing the closed loop transfer functions for these two controllers, it is easier to compare the magnitude of the sensitivity (Eq. 7), shown in Fig. 7(b). The sensitivity for Run 1418 shows disturbance amplification at 1650 Hz, which corresponds to the secondary tone found in the measured results. Disturbance amplification of nearly the same level is also predicted near 1500 Hz for Run 1418, but the measured results show very little amplification there. Near the third Rossiter mode at 1160 Hz, the sensitivity for the controllers is similar to one another, although the magnitude for Run 1418 is slightly higher than Run 1428 at 1200 Hz. This data suggests that Run 1418 should excite the upper sideband of the third Rossiter mode at least as much as Run 1428, but the measured results show this wasn't true.

Table 2 Control design parameters

Time (run #)	Mach #	# of states		Effort penalty parameters				Sensor Noise (dB)
		Full model	Reduced model	f_{min} (Hz)	f_{max} (Hz)	stopband (dB)	passband (dB)	
1355	0.275	199	80	500	1600	1	51	31
1428	0.35	160	60	400	1700	23	57	43
1535	0.45	195	60	400	2000	31	61	44
1418	0.35	160	60	300	2500	17	57	43

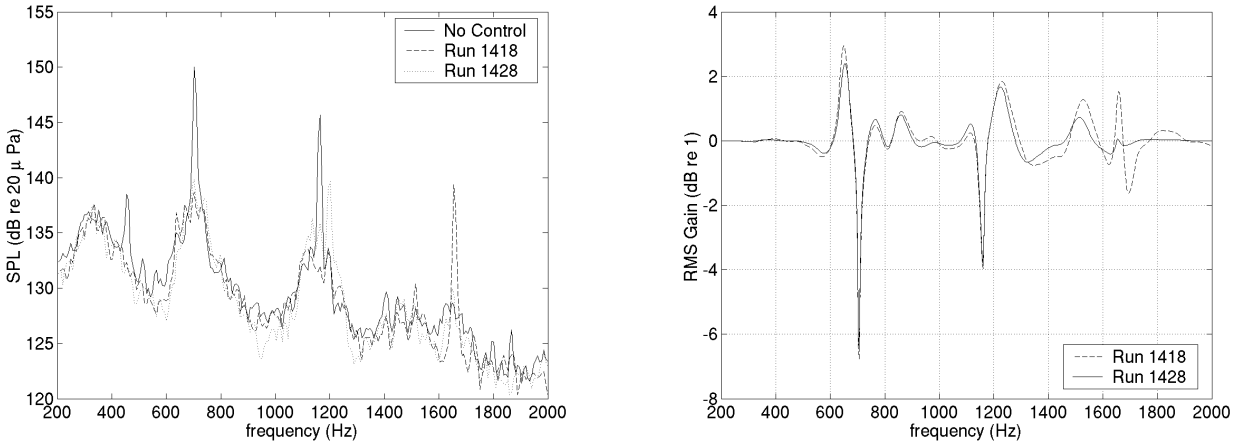

a) Measured performance, M=0.35.

b) Sensitivity, M=0.35.

Fig. 7 Control performance at Mach 0.35 and sensitivity

It is not known exactly why the sideband excitation of the two controllers was so different, but it may have been due to mode competition, where forced and natural frequencies compete for available energy in the shear layer. This competition between frequencies has been leveraged before in open and closed loop control configurations,[17,18] where the shear layer is driven with a secondary frequency in order to inhibit the natural feedback loop in the cavity. This non-linear interaction between frequencies will obviously not be predicted by linear models.

Results similar to those shown in Fig. 7 were observed in numerous closed loop control cases. Specifically, the closed loop performance of many controllers was limited by excitation of the sidebands of a Rossiter mode. Aggressive controllers which didn't excite the sidebands tended to create a secondary tone, like Run 1418. Some possible causes for this behavior are: inaccuracies in the identified plant model; side effects of high gain controllers and time delays in the plant; or, changes in the dynamics of the system once control is applied. A combination of these factors is also possible. Unfortunately, the current set of measurements is not sufficient to pinpoint the precise cause for the limitations in controller performance.

Conclusions

The application of discrete time linear quadratic control design methods using state space models computed from experimental data was demonstrated on the cavity tone problem. A synthetic jet actuator was located at the leading edge of the cavity, and two pressure transducers were mounted inside the cavity. The feedback control designs reduced multiple cavity tones at Mach 0.275, 0.35, and 0.45. General trends of disturbance amplification and attenuation found in the measured results agreed with predictions based on linear models.

Peak splitting and peaking were observed in some of the closed loop results. Peak splitting occurs when the controller increases the levels of sidebands near cavity tones; peaking refers to the generation of a secondary tone distinct from the cavity tones by the controller.

Although linear models of the cavity and closed loop system showed generally good agreement with measured results, the models do have limitations. For example, a linear model was shown to inadequately account for a strong tone at a high frequency affecting the dynamics at a lower frequency. Additional measurements are needed to better quantify the dynamics from actuator to sensor in the cavity.

References

[1]Huang, X. and Weaver, D., "On the Active Control of Shear Layer Oscillations Across a Cavity in the Presence of Pipeline Acoustic Resonance," *Journal of Fluids and Structures*, Vol. 5, 1991, pp. 207–219.

[2]Williams, D. R., Fabris, D., and Morrow, J., "Experiments on controlling multiple acoustic modes in cavities," *6th*

AIAA/CEAS Aeroacoustics Conference, No. AIAA-2000-1903, Lahaina, HI, June 2000.

[3]Williams, D. R. and Morrow, J., "Adaptive Control of Multiple Acoustic Modes in Cavities," *31st AIAA Fluid Dynamics Conference*, No. AIAA-2001-2769, Anaheim, CA, June 2001.

[4]Williams, D., Rowley, C., Colonius, T., Murray, R., MacMartin, D., Fabris, D., and Albertson, J., "Model-Based Control of Cavity Oscillations Part I: Experiments," *40th AIAA Aerospace Sciences Meeting and Exhibit*, No. AIAA-2002-0971, Reno, NV, Jan. 2002.

[5]Rowley, C., Williams, D., Colonius, T., Murray, R., MacMartin, D., and Fabris, D., "Model-Based Control of Cavity Oscillations Part II: System Identification and Analysis," *40th AIAA Aerospace Sciences Meeting and Exhibit*, No. AIAA-2002-0972, Reno, NV, Jan. 2002.

[6]Cattafesta III, L. and Garg, S., *Active Suppression of Shear-Layer/Cavity Resonance Interactions, Final Technical Report, Contract NAS2-14248*, NASA Ames Research Center, 1997.

[7]Cattafesta, L., Shukla, D., Garg, S., and Ross, J., "Development of an adaptive weapons-bay suppression system," *33rd AIAA Thermophysics Conference*, No. AIAA-99-1901, Norfolk, VA, May 1999.

[8]Venugopal, R. and Bernstein, D. S., "Adaptive Disturbance Rejection Using ARMARKOV/Toeplitz Models," *IEEE Transactions on Control Systems Technology*, Vol. 8, No. 2, March 2000, pp. 257–269.

[9]Anderson, B. and Moore, J., *Optimal Control - Linear Quadratic Methods*, Information and System Sciences Series, Prentice Hall, Englewood Cliffs, New Jersey, 1990.

[10]Mosca, E., *Optimal, Predictive, and Adaptive Control*, Prentice Hall, 1995.

[11]Juang, J.-N., *Applied System Identification*, Prentice Hall, 1994.

[12]Juang, J.-N., "State-Space System Realization with Input and Output Data Correlation," Tech. Rep. TP-3622, NASA Langley Research Center, April 1997.

[13]Rossiter, J., *Wind-Tunnel experiments on the flow over rectangular cavities at subsonic and transonic speeds*, Aeronautical Research Council Reports and Memoranda No. 3438, Oct. 1964.

[14]Heller, H., Holmes, D., and Covert, E., "Flow-induced pressure oscillations in shallow cavities," Tech. Rep. TR-70-104, AFFDL, Dec. 1970.

[15]Banaszuk, A., Mehta, P. G., Jacobson, C. A., and Khibnik, A. I., "Limits of Achievable Performance of Controlled Combustion Processes," *submitted to IEEE Transactions on Automatic Control*, 2001, Available from http://abanaszukresearch.homestead.com/files/preprintsgz.html.

[16]Saunders, W., Vaudrey, M., Eisenhower, B., Vandsburger, U., and Fannin, C., "Perspectives on Linear Compensator Designs for Active Combustion Control," *37th AIAA Aerospace Sciences Meeting and Exhibit*, No. AIAA-1999-0717, Reno, NV, Jan. 1999.

[17]Cattafesta III, L., Garg, S., Choudhari, M., and Li, F., "Active Control of Flow-Induced Cavity Resonance," *28th AIAA Fluid Dynamics Conference*, No. AIAA-97-1804, Snowmass Village, CO, June 1997.

[18]Shaw, L., "High Speed Application of Active Flow Control for Cavity Acoustics," *6th AIAA/CEAS Aeroacoustics Conference*, No. AIAA-2000-1926, Lahaina, HI, June 2000.